Title	60-GHz millimeter-wave identification reader on 90-nm CMOS and LTCC
Author(s)	Pursula, Pekka; Karttaavi, T.; Kantanen, Mikko; Lamminen, Antti; Holmberg, Jan; Lahdes, Manu; Marttila, Ilkka; Lahti, Markku; Luukanen, Arttu; Vähä-Heikkilä, Tauno
Citation	IEEE Transactions on Microwave Theory and Techniques vol. 59(2011):4, pp. 1166-1173
Date	2011
URL	http://dx.doi.org/10.1109/TMTT.2011.2114200
Rights	Copyright © 2011 IEEE. This article may be downloaded for personal use only

60-GHz Millimeter-Wave Identification Reader on 90-nm CMOS and LTCC

Pekka Pursula, *Member, IEEE*, Timo Karttaavi, Mikko Kantanen, Antti Lamminen, Jan Holmberg, Manu Lahdes, Ilkka Marttila, Markku Lahti, Arttu Luukanen, *Member, IEEE*, and Tauno Vähä-Heikkilä, *Member, IEEE*

***Abstract*—A reader module at 60 GHz for high data-rate short-range backscattering-based communications is presented. The reader consists of a CMOS-based oscillator, amplifiers, and a mixer on a low-temperature co-fired ceramic (LTCC) substrate. The filter, power splitter, and antennas are directly patterned on the LTCC. All millimeter-wave components are contained within the module and the only interfaces to the module are the IF and bias lines. Transmit power of the module is +11.6-dBm effective isotropic radiated power with an IF bandwidth of 400 MHz. The LTCC module measures 13 × 24 mm^2 and has a dc power consumption of 130 mW. Reception of a 20-MHz square wave from a tag 5 cm apart from the reader is demonstrated; the suggested millimeter-wave identification concept enables a 10^2–10^3-fold data-rate increase in comparison to the present near-field communication technique, with similar size, range, and power consumption of the reader.**

***Index Terms*—Backscattering modulation, CMOS, low-temperature co-fired ceramic (LTCC), millimeter-wave identification (MMID), monolithic microwave integrated circuit (MMIC), RF identification (RFID), 60 GHz.**

I. Introduction

THE development of wireless communications is driven by the need of higher communication bandwidths. The same trend is seen in cellular networks and wireless local area networks (WLANs), where consumer applications use more bandwidth, for example, video streaming. At the same time, mobile phones with near-field communication (NFC) capability are entering the market, enabling the user to access memory of an inexpensive transponder, or a tag, with a reader integrated in the mobile phone. However, the NFC technology only supports a data rate of 424 kbit/s at the 13.56-MHz band to a range of a few centimeters [1]. Many consumer applications would benefit if the data rate could be significantly increased, while keeping the data carrier, i.e., the tag, as inexpensive as possible.

Manuscript received May 27, 2010; revised January 14, 2011; accepted January 25, 2011. Date of publication March 10, 2011; date of current version April 08, 2011. This work was supported in part by Tekes (the Finnish funding agency for technology and innovation) under the Cooperative Traffic Project.

P. Pursula, M. Kantanen, A. Lamminen, J. Holmberg, M. Lahdes, I. Marttila, M. Lahti, A. Luukanen, and T. Vähä-Heikkilä are with the VTT Technical Research Centre of Finland, FI-02150 Espoo, Finland (e-mail: Pekka.Pursula@vtt.fi; Mikko.Kantanen@vtt.fi; Antti.Lamminen@vtt.fi; Jan.Holmberg@vtt.fi; Manu.Lahdes@vtt.fi; Ilkka.Marttila@vtt.fi; Markku.Lahti@vtt.fi; Arttu.Luukanen@vtt.fi; Tauno.Vaha-Heikkila@vtt.fi).

T. Karttaavi is with the Nokia Research Center, FI-00045 Helsinki, Finland (e-mail: timo.karttaavi@nokia.com).

Color versions of one or more of the figures in this paper are available online at http://ieeexplore.ieee.org.

Digital Object Identifier 10.1109/TMTT.2011.2114200

There are several technologies suggested for high data-rate short-range communications. Starting from the lowest carrier frequency, Gomez *et al.* [2] suggest updating the inductive communication used in NFC to 3.4 Mbit/s. A standardized technology exists at UHF, where RF identification (RFID) supports data rates up to 640 kbit/s [3]. Range of several meters is achieved with a 10 Euro-cent tag.

Ultra-wideband (UWB) technology has also been suggested for the application. Baghaei-Nejad *et al.* [4] report a low-power tag with 10-Mbit/s data rate based on a UWB uplink and UHF downlink. A different approach is taken in [5], where a passive tag at 60 GHz is described. The data rate is only 5 kbit/s, but the tag demonstrates power harvesting from the reader transmission with CMOS rectifier at 60 GHz. However, neither of these papers addresses the reader device. A tag alone is useless without a reader to access it. The intention of this work is to present a reader implementation with small size and low power consumption. Especially in handheld consumer devices, form factor and power consumption are decisive considerations.

In [6], the authors suggested using backscattering modulation at 60 GHz for high data-rate communications. The paper laid the theoretical grounds for the millimeter-wave identification (MMID), as well as presented experimental results with a waveguide-based reader device and a semipassive tag [7].

This paper presents an MMID reader that can be used for accessing tags, such as the one presented in [5] and [7]. The reader consists of CMOS components on a low-temperature co-fired ceramic (LTCC) substrate. Both of the technologies have potential for low cost in high volumes. LTCC technology offers stable and low-loss materials for millimeter waves and there has been a significant amount of research going on LTCC modules for 60-GHz point-to-point applications [8], [9]. Currently the highest frequency range where LTCC technology has been studied is 150 GHz [10].

The multilayer LTCC platform was chosen for the MMID reader modules because it allows direct integration of passive components such as antennas, power dividers, transmission lines, and filters. Furthermore, active components can also be flip-chip connected to the LTCC substrate. The oscillator, amplifiers [medium power amplifier (MPA) and low-noise amplifier (LNA)] and mixer are realized on 90-nm CMOS. All the millimeter-wave components are integrated to the module and only interfaces to the module are the IF ports and dc-bias lines.

Section II discusses the reader architecture in detail. Section III introduces the CMOS components. LTCC design component design and module integration is presented in Section IV. Finally, Section V presents measurement results from the reader module.

II. Reader Architecture

The MMID reader is very similar to a frequency-modulated continuous-wave (FMCW) radar. Both devices receive and detect the reflection of their own continuous transmission with some offset frequency. In the case of FMCW radar, the local oscillator (LO) frequency is swept and the offset frequency arises from time delay of the reflection, i.e., reflector distance. In the case of MMID, the LO is not swept, but the offset frequency is introduced by the transponder, which modulates its reflection to carry information.

The FMCW radar can be most easily implemented with a direct conversion architecture, which is also used in UHF RFID readers. A direct conversion FMCW radar module at 77 GHz is presented in [11]. The module is realized on SiGe and it uses external antennas on a printed circuit board (PCB).

In direct conversion architecture, the phase noise is correlated in the receiver (RX) mixer LO and RF ports for short reflector or transponder ranges [12]. Hence, the sensitivity is defined by the RX thermal noise. In FMCW radars, a delicate phase-locked loop (PLL) architecture is needed to achieve better linearity of the frequency sweep [13], but this is not required in MMID readers, where the LO frequency is not swept.

Heterodyne reception allows reducing the thermal noise bandwidth in FMCW radars, but is not as beneficial in MMID, where wide bandwidth is required for high data throughput. In addition to this, the phase noise correlation effect is lost due to separate LO signals in the transmitter (TX) and RX. However, this can be compensated with another IF frequency, as seen in [14], but the system is significantly more complex. The system complexity, especially the two LOs at millimeter waves, increases power consumption, which is not desired in the MMID reader for mobile applications.

Maximum transmitted power in a MMID reader, as well as an FMCW radar, is limited by the RX compression point and isolation between TX and RX antennas. The reflection from transponders is usually dominated by the direct near-field coupling from the TX to RX port. Active isolators, or reflection cancellers, have been designed for FMCW radars [12] and RFID readers at UHF [15], but at millimeter waves, high isolation can be achieved with separate TX and RX antennas even in a compact module.

The direct conversion architecture with a voltage-controlled oscillator (VCO) at 60 GHz is chosen for the MMID reader because it provides adequate sensitivity and output power with low component count and power consumption. The schematic of the MMID reader is presented in Fig. 1. The oscillator output is amplified using the MPA. The amplified signal is divided by a power splitter to the TX antenna array and to the LO port of the downconversion mixer. Another antenna array is utilized for receiving the signal from an MMID tag. The received signal is amplified using the LNA and fed to the RF port of the mixer.

A. Read Range

Let us estimate the read range and data bandwidth available for an MMID system. The signal incident to the reader RX is generated in a MMID tag by backscattering modulation.

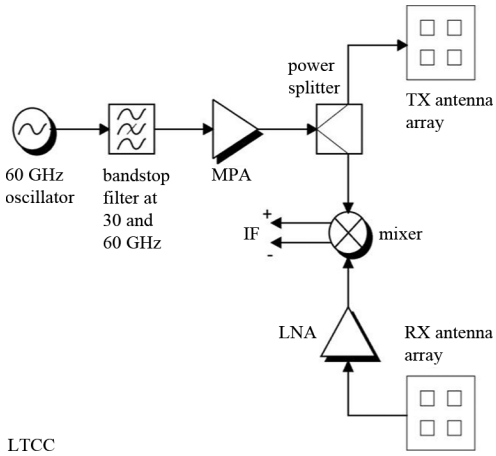

Fig. 1. Block diagram of the MMID reader. Shaded components are implemented on silicon, others are integrated to the LTCC.

Reference [6, Eq. (6)] can be utilized to calculate the modulated radar cross section for a tag

$$\sigma_m = \frac{G_A^2\lambda^2}{16\pi}\left|\Gamma_1 - \Gamma_2\right|^2 = \frac{G_A^2\lambda^2}{4\pi}m \tag{1}$$

where G_A is the tag antenna gain and $m = |\Gamma_1 - \Gamma_2|^2/4$ is the modulation coefficient. The power incident to the reader RX is

$$P_{\rm rx} = P_{\rm tx}\left[\frac{\lambda^2 G_{\rm rx}G_{\rm tx}\sigma_m}{(4\pi)^3 d^4} + L_{\rm tx/rx}\right] \tag{2}$$

where $G_{\rm rx}$ and $G_{\rm tx}$ are the RX and TX antenna gain, respectively, $P_{\rm tx}$ is the transmit power, d is the distance between the tag and the reader, and $L_{\rm tx/rx}$ is the isolation from the TX antenna port to RX antenna port. The first term describes the information carrying reflection from the transponder and the second is the direct coupling from TX to RX antenna ports. The first term is -44 dB for $G_{\rm rx} = G_{\rm tx} = G_a = 10$ dB, $d = 5$ cm, and $m = 1$. Hence, the input power is usually dominated by the direct near field coupling of the TX and RX antennas.

Let us assume that the RX is in the linear operation range, i.e.,

$$L_{\rm tx/rx} < \frac{P_{1\ \rm dB}}{P_{\rm tx}} \tag{3}$$

where $P_{1\ \rm dB}$ is the RX input compression point. Now the resolution of the RX is defined by the RX white noise because phase noise in the LO and RF ports of the downconversion mixer are correlated. Hence, we can calculate the noise power at the input as [16]

$$P_n = kT \cdot {\rm BW} \cdot F \tag{4}$$

where k is the Boltzmann constant, T is the absolute temperature, BW is the IF bandwidth, and F is the noise factor. The signal-to-noise ratio (SNR) is given by

$${\rm SNR} = \frac{P_{\rm tx}}{kT \cdot {\rm BW} \cdot F}\frac{\lambda^2 G_{\rm rx}G_{\rm tx}\sigma_m}{(4\pi)^3 d^4} \tag{5}$$

which relates transmit power to noise power and communication range. For an estimation of the available data bandwidth, the BW can be solved from (5) for a fixed SNR. To maximize the SNR, the device should minimize the reader noise factor and

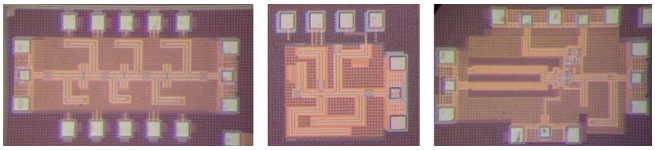

Fig. 2. Photographs of the CMOS components (from left to right): LNA (0.65×1.2 mm^2), oscillator (0.7×0.7 mm^2), and mixer (1.1×0.7 mm^2).

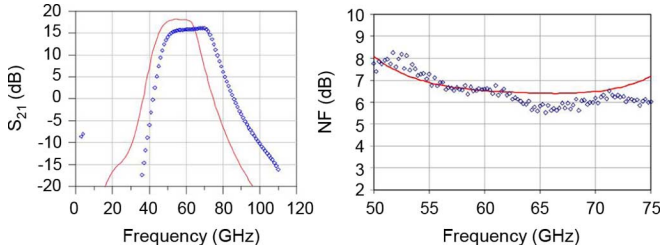

Fig. 3. Measured (dots) and simulated (solid) gain (*left*) and noise figure (*right*) of the LNA [17].

maximize the output power, keeping in mind the linearity requirement in (3). The following sections will first introduce the CMOS components and then the design of the LTCC module in accordance to these objectives is presented.

III. CMOS Components

The integrated circuits were fabricated in STMicroelectronics 90-nm bulk CMOS technology. Seven copper metal layers were available with the two topmost layers thicker than the others. Dedicated metal–insulator–metal (MIM) capacitor processing was not used since it may not be available when striving for the best possible cost efficiency with a basic digital process option.

Transistor layout and the details of the access geometry were optimized by fabricating test structures. In this case, we used nMOS devices with 80 parallel 1-μm-wide fingers (total gatewidth 80 μm) to minimize the gate resistance. Our measurements indicate a transition frequency f_t of 140 GHz and $f_{\max}$ of approximately 200 GHz for the 80-μm device. The BSIM3 model supplied by the foundry was used in the nonlinear simulations with added external parasitics to match the measured behavior of the test devices. A small-signal model was constructed using S-parameter measurements up to 110 GHz and noise parameter measurements at 50-75 GHz. Similarly, test structures were made to characterize different passive structures. Loss for a 50-Ω coplanar waveguide (CPW) was measured to be approximately 15 dB/cm ($\lambda = 2.3$ mm). The specific capacitance of stacked finger capacitors on five metal layers was found similar to the optional MIM capacitors.

Four active blocks were designed: an LNA, an MPA, an oscillator, and a mixer. The die photographs of the devices are shown in Fig. 2.

A. Amplifiers

The amplifier designs are based on a traditional MMIC approach where transmission lines are used for reactive matching in the input, output, and inter-stage matching circuits [17]. Transistor bias voltages are connected through (RF) short-circuited stubs. To avoid very short short-circuited (inductive) transmission lines, shunt capacitors were used instead for matching. Finger capacitors consisting of five bottom metal layers were used for this as well as for dc blocking and RF shorting. Inductive source degeneration was used in all three stages to improve stability.

The amplifier S-parameters were measured on-wafer using a vector network analyzer. Fig. 3 shows the measured and simulated gain and noise figure of the LNA. The measured maximum gain is 16 dB and input compression point -9 dBm.

The measured gain shows a shift upward in frequency. This shift notwithstanding, the correspondence between the curves is good. A simple explanation for this could be an error in transmission line models. Indeed, by tuning the effective dielectric constant $\varepsilon_{r,\mathrm{eff}}$ of all the lines by a constant amount, the fit becomes remarkably good. The noise figure of the LNA was measured on-wafer using a system based on V-band waveguide components. A Y-factor method was utilized with a calibrated solid-state noise source and a down-converting RX. The measured noise figure at 60 GHz is 7 dB.

A similar two-stage amplifier with a slightly larger output device was used to design an MPA. The gain and saturated output power of the MPA are 9 dB and 8 dBm, respectively.

B. Oscillator

Transmission lines, instead of *LC* tanks, were used as resonators to avoid the need for inductors and high-quality capacitors. A single transistor in a common-gate configuration was used as a negative-resistance two-port for the oscillator core [18]. Negative resistance generation was optimized by adding an inductive shorted transmission line on the gate. Drain and source ports were terminated with resonator impedances that fulfill the oscillation startup conditions. Drain and gate bias voltages are connected through low-impedance points in the resonator stubs (at an RF short). The bias lines also include some filtering to suppress parasitic low-frequency oscillation modes. In this application, the oscillator was used in a free-running configuration.

The oscillating frequency, output power, and phase noise were measured on-wafer using an Agilent E4407B spectrum analyzer. An external harmonic mixer was used for downconverting the signal to the analyzer operating band. The measured output power is -3 dBm. Power consumption of the oscillator is 25 mW from a 1-V supply voltage. The single sideband (SSB) phase noise level is approximately -85 dBc/Hz at 1-MHz offset.

C. Mixer

In microwave applications, resistive mixers [19], [20] have recently become quite popular due to simpler structure and typically lower power consumption compared to, for example, classic Gilbert cell mixers. The designed resistive downconversion mixer for the RX consists of a mixer core, a buffer amplifier, and a Marchand balun in the LO input port [21]. The buffer amplifier provides differential baseband or low IF signal. The RF signal is fed into the sources and balanced LO to the zero biased gates. The buffer amplifier is a balanced cascade of

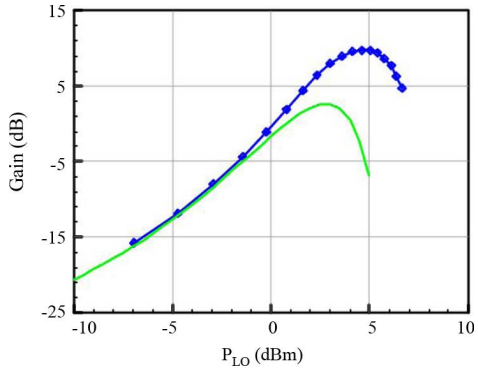

Fig. 4. Measured (dots) and simulated conversion gain at 60 GHz [21].

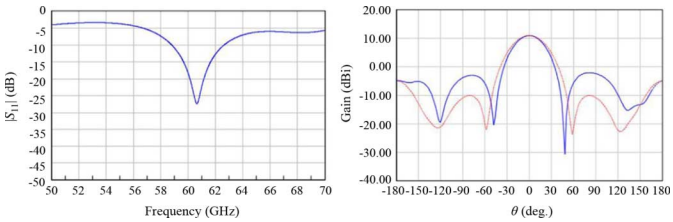

Fig. 5. Simulations on the 2×2 antenna array: Reflection coefficient (*left*) and gain at 60 GHz (*right*): E-plane (solid) and H-plane (dotted) patterns.

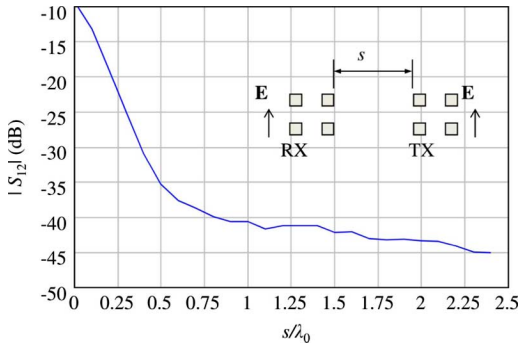

Fig. 6. Simulated mutual coupling between the RX and TX arrays in the H-plane as a function of spacing between the outermost array elements.

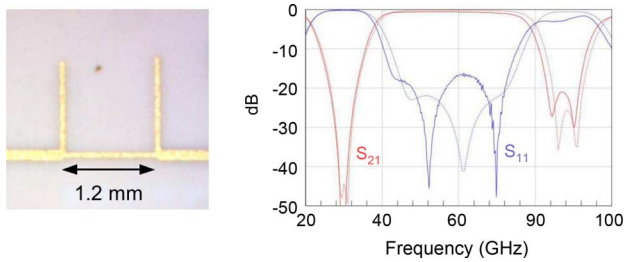

Fig. 7. Bandstop filter: photograph (*left*). Simulated (dotted) and measured (solid) reflection coefficients S_{11} and S_{21} (*right*).

source follower and common source stages. CPWs are used as transmission lines.

The measured and simulated differential conversion gains versus LO level are shown in Fig. 4. The deviation is less than one decibel for LO levels under 0 dBm.

The measured differential one decibel compression point $P_{1\ \mathrm{dB}}$ is -2 dBm, which is enough for this application. The optimum RF-port matching occurs at about 10-GHz lower frequency than anticipated, but the return loss is still better than -10 dBm around 60 GHz. The baseband bandwidth of the circuit is over 400 MHz. The measured LO to RF port isolation is about 34 dB and noise figure is about 27 dB.

IV. LTCC Components

A. Antenna Arrays

Planar 2×2 RX and TX antenna arrays were designed on the LTCC board. The idea was to have small and compact antennas without sacrificing the gain and bandwidth. The arrays are similar to the one shown in [22, Fig. 5] but four array elements were used instead of 16. Wilkinson power dividers were used in the feed network.

Simulated (HFSS) matching and gain patterns of the 2×2 array are presented in Fig. 5. The -10-dB frequency band is 58.8–62.6 GHz, indicating the impedance bandwidth of 6.3%. The maximum gain is 11.1 dBi at 61 GHz.

The mutual coupling between the TX and RX antenna arrays should be minimized to guarantee the designed system functionality. The mutual coupling of rectangular microstrip antennas is stronger in the E-plane than in the H-plane [23]. Hence, the arrays were placed side by side along the H-plane.

The array separation s depends on the needed isolation between the RX and TX arrays (Fig. 6). It is seen that with separation larger than about two wavelengths, the coupling remains almost constant. With the chosen value of separation, $s = 10$ mm $(2\lambda_0)$, the mutual coupling is about $L_{\mathrm{tx/rx}} = -43$ dB, same order of magnitude than the reflection from a tag at a distance of 5 cm [see (2)]. In comparison, using a rat-race coupler with a common TX/RX antenna, the coupling between TX and RX ports was measured to be 20 dB in the FMCW radar at 77 GHz presented in [11].

B. Filters

A filter between the oscillator and amplifier was required to remove the oscillator harmonics at 30 and 90 GHz. A second-order Chebyshev bandstop filter was selected for the application. The filter is directly patterned to the LTCC. Fig. 7 presents the layout and the simulated and measured S-parameters of the filter. Measured isolation is better than 40 dB at 30 GHz and better than 20 dB at 90 GHz. Measured insertion loss at 60 GHz is less than 1 dB.

C. LTCC Technology and Assembly

The reader module is realized on an LTCC platform, which consists of four layers (see Fig. 8). The thickness of the module is about 400 μm. Antenna arrays are integrated on the LTCC, as well as power splitters and filters. Interconnections between the components utilize 50-Ω microstrip lines. IF output and bias connections are routed to the PCB using ball grid array (BGA) connections on the component side of the LTCC. Differential IF is fed to two SMA connectors on the carrier substrate and a 15-pin D-connector is used as a bias connector.

The Ferro A6-M system was selected for this study due to its good high-frequency properties. The relative permittivity of

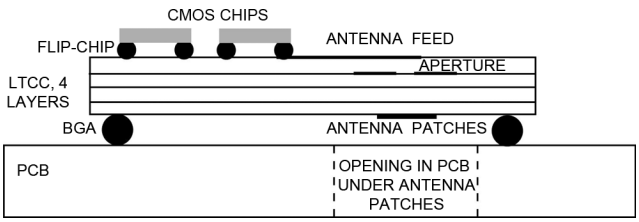

Fig. 8. Schematic view of the reader module based on the LTCC technology. CMOS components are flip chipped to an LTCC substrate, which also contains antenna arrays, filters, power dividers, and other passives. The LTCC module is connected to a PCB with a BGA.

the dielectric was 5.74 at 60 GHz and loss tangent at 0.0023. The system utilizes screen-printed gold (Au) conductors with the conductivity of 2.5×10^7 S/m. The material properties stay quite constant over a wide frequency range. Instead, the millimeter-wave performance of the LTCC modules is mainly affected by processing issues such as linewidth variations due to printing steps or shrinkage during firing [24].

In LTCC technology, the processing is started by punching and filling of via-holes. The conductors are then screen-printed individually onto each sheet. The minimum linewidth is 100 μm with a typical tolerance of 5%. Cavities for MMICs are punched before tape layer stacking. Interlayer alignment accuracy of 10–15 μm is achieved using registration pins. Silicone inserts are molded into the cavities to keep the shape of the cavities during lamination. In this work, the lamination pressure was 3000 psi and the temperature was 70 °C, specific to the Ferro A6-M LTCC system. The silicone inserts are carefully removed after the lamination. The process is completed by co-firing at the peak temperature of about 850 °C.

At millimeter waves, the assembly methods have to be considered carefully. Flip-chip interconnections eliminate the parasitic inductances caused by bonding wires. If the flip-chip process is not feasible in some cases, ribbon bonding can be used instead of conventional wire-bonding. In this work, flip-chipping is based on Au stud bumps. The diameter of the bumps is about 60 μm and the height is about 20 μm. The flip-chip process utilizes a thermo-compression method. Bonding force and temperature has to be optimized for each component.

The final step in the assembly process is the BGA soldering. A compromise between the high-frequency properties and reliability has to be made when the diameter of the BGA ball is selected [25]. In this case, 850-μm BGA balls (10/90 SnPb) were attached with an SnAg (96/4) solder onto the bottom side of the substrate in a reflow oven at the peak temperature of 260 °C. The module was then reflow-soldered onto a PCB using an SnCu-alloy solder, which was melted at the peak temperature of 235 °C. Photographs of the complete LTCC module are presented in Fig. 9.

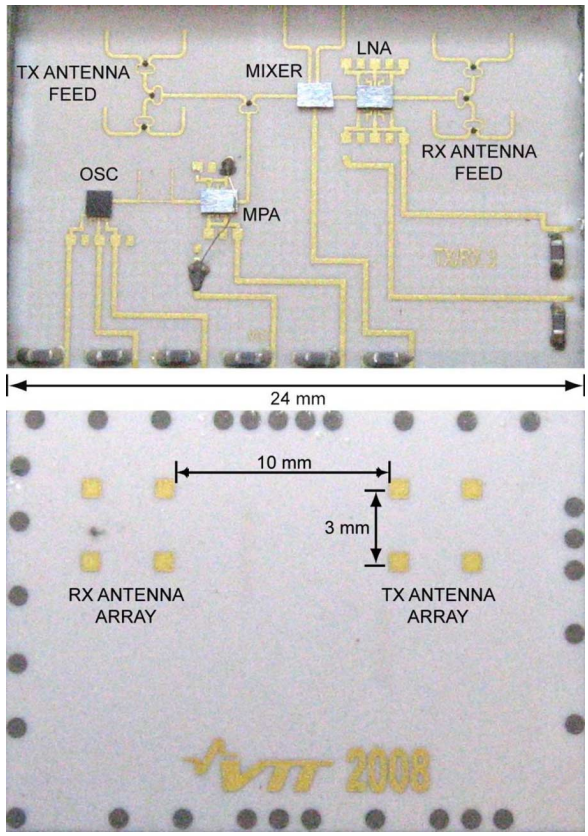

Fig. 9. Photographs of the LTCC module. The component side (above) and the antenna side (below). Module measures 24 × 13 mm^2.

V. Experimental Results

A. Output Power and Input Compression

Both the transmit power and RX conversion gain were measured with transmission method. The measured transmit power is 11.6-dBm EIRP. The LO delivers a power of −3 dBm and the TX chain has a gain of 17 dB (9 dB from the MPA, −3 dBm from the power divider, and 11 dB from the antenna). Hence, the measured overall TX power is 2.4 dB lower than estimated from component values only. However, the TX chain also includes several millimeters of transmission lines and flip-chip connections, as well as the filter, which, together, can explain the additional attenuation.

The power fed to the TX antenna can be estimated to be $P_{\rm tx} = 0.6$ dBm (in comparison, 2 dBm with SiGe at 77 GHz in [11]). The simulated direct coupling between the TX antenna and RX antenna ports is $L_{\rm tx/rx} = -43$ dB. Hence, the carrier power incident to the RX is around −40 dBm. The RX compression is defined by the mixer input compression point, which is −2 dBm, resulting in RX input compression point of −18 dBm, which is 10 dB less than the input compression point of the LNA alone. The RX should be well in its linear operation region for transponders and reflectors farther than about 50 mm away. Below that distance, the reflection from the transponder starts to dominate over direct coupling and saturation may occur.

The reader dc power consumption was measured to be 130 mW. Using a commercial GaAs-based MPA, LNA, and mixer components [26] in the same architecture, the system output power and noise figure would be approx. 18-dBm EIRP and 4 dB, respectively. However, the power consumption would be more than fourfold, 160 mW by the LNA and 400 mW by the MPA, which is too much for a mobile application.

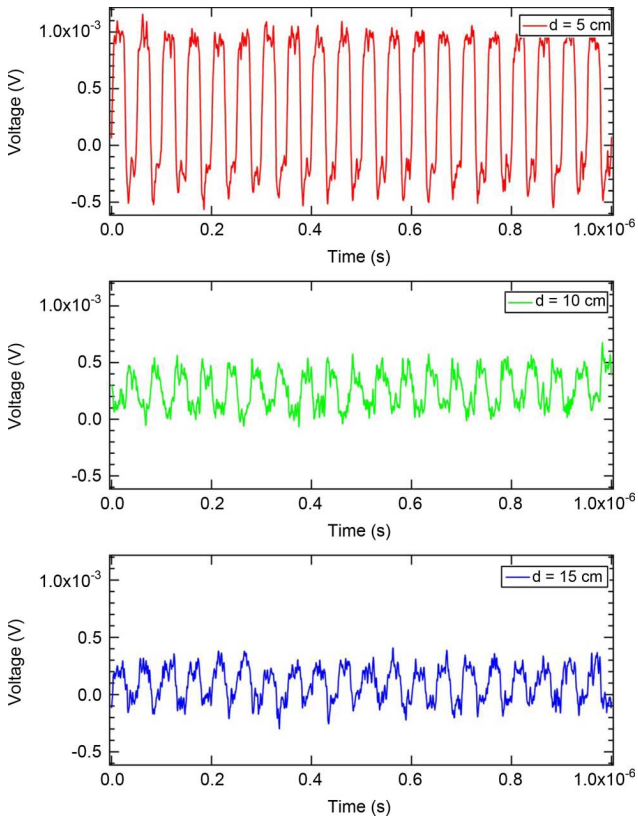

Fig. 10. Received IF signals for different communication ranges d.

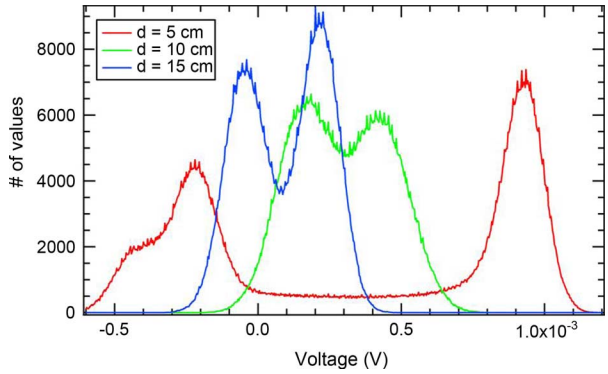

Fig. 11. Histograms of the received time-domain signals at different operation distances d.

TABLE I
MEASURED RX SIGNAL AND NOISE

d (cm)	V_{rx} (mV)	V_n (mV)	SNR (dB)
5	0.57	0.075	17.7
10	0.13	0.10	2.6
15	0.13	0.074	4.8

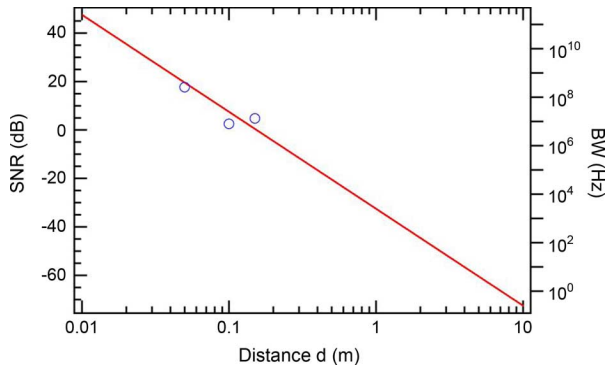

Fig. 12. Calculated (lines) and measured (dots) SNR as a function of operation distance. The available bandwidth (BW) as a function of the operation distance is calculated based on the measurements.

B. Read Range and SNR

In Fig. 10, the IF signal from the reader is shown for an MMID tag at three different distances d. The tag modulates its backscattering by a 20-MHz square wave and the IF bandwidth is 400 MHz, limited by the downconversion mixer.

The SNR of the system is estimated by taking histograms of the signal voltages. The histograms in Fig. 11 are created from a time-domain signal of 200 μs, which consists of 1 Msamples. The peaks are Gaussian, except for the lower peak at the nearest distance $d = 5$ cm, which can be explained by fitting two Gaussian peaks to it. Also, all the peaks are roughly equally wide, independent of the communication range, i.e., the backscattered signal power. Gaussian power-independent characteristics imply that the noise is dominated by the RX white noise.

Signal root mean square (rms) voltage $V_{\rm rx}$ is half of the peak separation in the histogram and noise rms voltage is given by the width of the peak; more precisely, a Gaussian function is fitted to each peak and the standard deviations of the two peaks at each operation distance are averaged to get the noise rms voltage V_n. Table I presents the signal and noise at different communication ranges.

The noise is almost constant with range, as it should be for RX white noise. The signal, however, is almost the same for distances 10 and 15 cm, which can be either due to multipath propagation, or due to antenna near-field coupling; The antennas are too near each other to fully validate the use of Friis or radar equations.

The measured noise varies from point to point and is 12.2–14.8 dB higher than the thermal noise of a 50-Ω load with $\mathrm{BW} = 400$ MHz, i.e., the noise figure of the RX is about 12.2–14.8 dB. The noise figure estimated from the LNA and mixer characteristics is 12.4 dB. Hence, the measured noise figure of the RX is a few decibels higher than estimated from component values only. The difference can be explained by additional losses due to transmission lines and flip-chip connections, as well as the low driver LO power of the mixer.

Fig. 12 presents the measured and calculated SNR as a function of tag distance. The SNR is calculated using (5). The measured values fit well to calculated ones with $\mathrm{BW} = 400$ MHz, $\mathrm{NF} = 12.2$ dB, and $m = 0.01$. The available data bandwidth was also estimated using (5) with a constant $\mathrm{SNR} = 17.7$ dB. The measured result at $d = 5$ cm presents the bandwidth of 400 MHz, which is the IF bandwidth of the downconversion mixer. The available bandwidth scales as d^{-4}, as does the SNR. A longer range can be achieved with lower bandwidth, or with a higher modulation index of the tag. On the other hand, at very low distances, a very high bandwidth is available.

VI. Conclusion

This paper has presented an MMID reader at 60 GHz. The reader consists of a CMOS oscillator, amplifiers, and a mixer on an LTCC substrate, on which filters, power dividers, and antenna arrays are directly fabricated. All the millimeter-wave components are included in the module and only IF and bias connections are contacted to the supporting PCB.

All the individual components, as well as the whole system, were introduced. The characteristics of the whole system were measured and compared to the characteristics of the individual components and found to be in good agreement with each other. The reader transmit power is 11.6-dBm EIRP and IF bandwidth is 400 MHz. The range and available communication bandwidth of a system containing the reader and a semipassive tag was estimated. At 5 cm, a $\mathrm{BW} = 400$ MHz was demonstrated with $\mathrm{SNR} = 17.7$ dB. The bandwidth is 10^2–10^3 higher than in NFC, where backscattering modulation is used at 424 kb/s with a similar range. Furthermore, the power consumption (130 mW) and the size $(13 \times 24\ \mathrm{mm}^2)$ of the MMID reader module are comparable to those of an NFC reader.

References

[1] "NFC Forum device requirements 1.0," NFC Forum Inc., Wakefield, MA, 2010. [Online]. Available: http://www.nfc-forum.org/

[2] B. Gomez, G. Masson, P. Villard, G. Robert, F. Dehmas, and J. Reverdy, "A 3.4 Mb/s RFID front-end for proximity applications based on a delta-modulator," in *Solid-State Circuits Conf.*, San Francisco, CA, Feb. 6–9, 2006, pp. 1211–1217.

[3] "EPC radio-frequency identity protocols, class-1 generation-2 UHF RFID, protocol for communications at 860 MHz–960 MHz, version 1.2.0" EPCglobal Inc., 2008. [Online]. Available: http://www.gs1.org/epcglobal/

[4] M. Baghaei-Nejad, H. Tenhunen, and Z. Li-Rong, "Power management and clock generator for a novel passive UWB tag," in *Int. System-on-Chip Symp.*, Tampere, Finland, Nov. 20–21, 2007, pp. 1–4.

[5] S. Pellerano, J. Alvarado, and Y. Palaskas, "A mm-wave power harvesting RFID tag in 90 nm CMOS," in *Custom Integr. Circuits Conf.*, San Jose, CA, Sep. 13–16, 2009, pp. 677–680.

[6] P. Pursula, T. Vähä-Heikkilä, A. Müller, D. Neculoiu, G. Konstantinidis, A. Oja, and J. Tuovinen, "Millimetre wave identification—new radio system for low power, high data rate and short range," *IEEE Trans. Microw. Theory Tech.*, vol. 56, no. 10, pp. 2221–2228, Oct. 2008.

[7] D. Neculoiu, G. Konstantinidis, T. Vähä-Heikkilä, A. Müller, D. Vasilache, A. Stavinidris, L. Bary, M. Dragoman, I. Petrini, C. Buiculescu, Z. Hazoupulos, N. Kornilios, P. Pursula, R. Plana, and D. Dascalu, "GaAs membrane-supported 60 GHz receiver with Yagi-Uda antenna," in *8th Int. RF MEMS and RF Microsyst. Symp.*, Barcelona, Spain, Jun. 26–29, 2007, pp. 15–18.

[8] J.-H. Lee, S. Pinel, J. Papapolymerou, J. Laskar, and M. Tentzeris, "Low-loss LTCC cavity filters using system-on-package technology at 60 GHz," *IEEE Trans. Microw. Theory Tech.*, vol. 53, no. 12, pp. 3817–3824, Dec. 2005.

[9] Y. Zhang, M. Sun, K. Chua, L. Wai, and D. Liu, "Antenna-in-package design for wirebond interconnection to highly integrated 60-GHz radios," *IEEE Trans. Antennas Propag.*, vol. 57, no. 10, pp. 2842–2852, Oct. 2009.

[10] A. Khalil, D. Passerieux, S. Verdeyme, L. Rigaudeau, and D. Baillargeat, "150 GHz bandpass filter using LTCC technology," *IEEE Microw. Wireless Compon. Lett.*, vol. 19, no. 7, pp. 455–457, Jul. 2009.

[11] R. Feger, C. Wagner, S. Schuster, S. Scheiblhofer, H. Jager, and A. Stelzer, "A 77-GHz FMCW MIMO radar based on an SiGe single-chip transceiver," *IEEE Trans. Microw. Theory Tech.*, vol. 57, no. 5, pp. 1020–1035, May 2009.

[12] A. G. Stove, "Linear FMCW radar techniques," *Proc. Inst. Elect. Eng.—Radar Signal Process.*, vol. 139, no. 5-F, pp. 343–350, Oct. 1992.

[13] C. Wagner, A. Stelzer, and H. Jager, "PLL architecture for 77-GHz FMCW radar systems with highly-linear ultra-wideband frequency sweeps," in *IEEE MTT-S Int. Microw. Symp. Dig.*, San Francisco, CA, Jun. 11–16, 2006, pp. 399–402.

[14] K. B. Cooper, R. J. Dengler, G. Chattopadhyay, E. Schlecht, J. Gill, A. Skalare, I. Mehdi, and P. H. Siegel, "A high-resolution imaging radar at 580 GHz," *IEEE Microw. Wireless Compon. Lett.*, vol. 18, no. 1, pp. 64–66, Jan. 2008.

[15] P. Pursula, M. Kiviranta, and H. Seppä, "UHF RFID reader with reflected power canceller," *IEEE Microw. Wireless Compon. Lett.*, vol. 19, no. 1, pp. 48–50, Jan. 2009.

[16] H. Nygvist, "Thermal agitation of electric charges in conductors," *Phys. Rev.*, vol. 32, pp. 110–113, 1928.

[17] T. Karttaavi, M. Kantanen, and J. Holmberg, "Transistor noise modeling for a 60 GHz CMOS LNA," in *Proc. Global Millimeter Waves Symp.*, Incheon, Korea, Apr. 14–16, 2010, pp. 307–310.

[18] M. Kantanen, J. Holmberg, T. Karttaavi, and J. Volotinen, "60 GHz receiver circuits using 90 nm CMOS," in *Proc. Joint 5th ESA Millimetre Wave Technol. Appl. Workshop/31st ESA Antenna Workshop*, Noordwijk, The Netherlands, 2009, pp. 311–318.

[19] F. Ellinger, "26.5–30 GHz resistive mixer in 90 nm VLSI SOI CMOS technology with high linearity for WLAN," *IEEE Trans. Microw. Theory Tech.*, vol. 53, no. 8, pp. 2559–2565, Aug. 2005.

[20] F. Ellinger, L. C. Rodoni, G. Sialm, C. Kromer, G. von Büren, M. L. Schmatz, C. Menolfi, T. Toifl, T. Morf, M. Kossel, and H. Jäckel, "30–40 GHz drain-pumped passive mixer MMIC fabricated on VLSI SOI CMOS technology," *IEEE Trans. Microw. Theory Tech.*, vol. 52, no. 5, pp. 1382–1391, May 2004.

[21] M. Kantanen, J. Holmberg, T. Karttaavi, and J. Volotinen, "60 GHz frequency conversion 90 nm CMOS circuits," in *Proc. EuMIC 2008*, Amsterdam, The Netherlands, Oct. 27–28, 2008, pp. 60–63.

[22] A. E. I. Lamminen, J. Säily, and A. R. Vimpari, "60-GHz patch antennas and arrays on LTCC with embedded-cavity substrates," *IEEE Trans. Antennas Propag.*, vol. 56, no. 9, pp. 2865–2874, Sep. 2008.

[23] D. M. Pozar, "Input impedance and mutual coupling of rectangular microstrip antennas," *IEEE Trans. Antennas Propag.*, vol. AP-30, no. 6, pp. 1191–1196, Nov. 1982.

[24] V. Kondratyev, M. Lahti, and K. Kautio, "On the LTCC characterization in millimeter-waves," in *40th Eur. Microw. Conf.*, Paris, France, Oct. 1, 2010, pp. 156–159.

[25] T. Kangasvieri, J. Halme, J. Vähäkangas, and M. Lahti, "Low-loss and broadband BGA package transition for LTCC-SiP applications," *Microw. Opt. Technol. Lett.*, vol. 50, pp. 1036–1040, 2008.

[26] "Datasheets of HMC-ABH209, HMC-ALH382, HMC-MDB169," Hittite Microw. Corporation, Chelmsford, MA, 2010. [Online]. Available: http://www.hittite.com

Pekka Pursula (M'09) was born in Vantaa, Finland, in 1978. He received the M.Sc. degree (with distinction) and D.Sc. in technical physics from the Helsinki University of Technology (TKK), Espoo, Finland, in 2002 and 2009, respectively.

In 2002, he was with Philips Medical Systems Finland, where he developed RF systems in magnetic resonance imaging (MRI). Since 2003, he has been with the VTT Technical Research Centre of Finland, Espoo, Finland, where he is currently a Senior Research Scientist. He has authored or coauthored over 20 peer-reviewed journal and conference papers. His research interests include RFID systems at UHF and millimeter waves, as well as wireless sensors.

D.Sc. Pursula was the recipient of the 2004 Young Scientist Award of the URSI/IEEE XXIX Finnish Convention on Radio Science.

Timo Karttaavi received the degree of M. Sc. (EE) and Lic. Sc. (EE) from the Helsinki University of Technology (TKK), Espoo, Finland, in 1989 and 2000, respectively.

His professional experience includes working with the Radio Laboratory, Helsinki University of Technology (1987–1989) and the Electromagnetics and Acoustics Laboratory, cole Polytechnique Federale de Lausanne, Switzerland (1990–1991 academic year). From 1991 to 1993, he was with the University of Helsinki, where he was involved with

particle detector read-out electronics stationed at CERN, Geneva, Switzerland. From 1993 to 2008, he was with the Technical Research Centre of Finland (VTT), where he was involved with microwave and millimeter-wave circuit and system research. This included a period with the Berkeley Wireless Research Center (2005–2006) during which time he was involved with millimeter-wave CMOS circuit design. In 2008, he joined the Nokia Research Center, Helsinki, Finland, where he is currently involved in radio system research.

Mikko Kantanen received the M.Sc. (Tech.) and Lic.Sc. (Tech.) degrees in electrical engineering from the Helsinki University of Technology (TKK), Espoo, Finland, in 2001 and 2006, respectively, and is currently working toward the Ph.D. degree at the Helsinki University of Technology.

Since 2001, he has been with the VTT Technical Research Centre of Finland, Espoo, Finland, where he is currently a Senior Research Scientist. His research interests include millimeter-wave integrated-circuit design, millimeter-wave measurements, and millimeter-wave systems.

Mr. Kantanen was a corecipient of an Asia–Pacific Microwave Conference 2006 Prize.

Antti Lamminen was born in Lappajärvi, Finland, in 1980. He received the M.Sc. (Tech.) degree in electrical engineering from the Helsinki University of Technology, Espoo, Finland, in 2006.

Since 2005, he has been with the VTT Technical Research Centre of Finland, Espoo, Finland, initially as a Research Trainee, and since 2006, as a Research Scientist. His current research interests include beam-steerable millimeter-wave antenna arrays, electrically small antennas, and electromagnetic modeling.

Jan Holmberg was born in Mäntsälä, Finland, in 1953. He received the M.Sc. degree in electrical engineering from the Helsinki University of Technology (TKK), Espoo, Finland, in 1978.

From 1977 to 1979, he was with the Acoustics Laboratory, TKK. From 1980 to 1981, he was with Kari Pesonen Consulting Engineers. Since 1982, he has been a Research Scientist and subsequently a Senior Research Scientist with the VTT Technical Research Centre of Finland, Espoo, Finland. Since 1985, he has been a Lecturer with the Circuit Theory Laboratory, TKK, teaching a course on active filters. His current research interests are the design of integrated analog circuits and active circuit theory.

Mr. Holmberg is a member of the Audio Engineering Society, Acoustical Society of Finland, and the Finnish Society of Electronics Engineers.

Manu Lahdes received the M.Sc. degree in electrical engineering from the Helsinki University of Technology (TKK), Espoo, Finland, in 1996.

He has authored or coauthored several papers. His research interests concern the millimeter-wave area and include on-wafer noise parameter measurements, cryogenic on-wafer measurements, active device modeling, and MMIC design and testing. His current activities also include passive millimeter imaging, integrated circuit design and modeling, and LTCC and microelectromechanical systems (MEMS) design.

Ilkka Marttila was born in Punkalaidun, Finland, in 1956. He received the M.Sc. degree in electrical engineering from the Helsinki University of Technology (TKK), Espoo, Finland, in 1982.

From 1981 to 1984, he was a Research Scientist with the Helsinki University of Technology. Since 1984, he has been with the VTT Technical Research Centre of Finland, Espoo, Finland, where his main research interests have been satellite communications and other RF electronics including theory and practice.

Markku Lahti received the M.Sc. and D.Sc. degrees in electrical engineering from the University of Oulu, Oulu, Finland, in 1993 and 2008, respectively.

In 2001, he joined the VTT Technical Research Centre of Finland, Espoo, Finland, where he is currently a Senior Research Scientist. His research interests include packaging of ceramic and polymer modules.

Arttu Luukanen (M'05) was born in 1972. He received the M.Sc. degree (hons) in applied physics from the University of Helsinki, Helsinki, Finland, in 1999, and the Ph.D. degree (hons) in applied physics from the University of Jyväskylä, Jyväskylä, Finland, in 2003.

From 2003 to 2005, he was a Guest Researcher with the National Institute of Standards and Technology, Boulder, CO. In 2005, he became the Director of the MilliLab—the Millimetre-wave Laboratory of Finland. In 2009, he was nominated as a Research Professor on Micro and Nanosystems with the VTT Technical Research Centre of Finland, Espoo, Finland. Since 2007, has served on the International Advisory Board of the FOI-FOCUS Centre of Excellence on Sensors, Multisensors and Sensor networks. He has authored or coauthored over 30 peer-reviewed journal and conference papers and several patents related to terahertz imaging with microbolometric detectors.

Dr. Luukanen is a member of the Finnish Academy of Technical Sciences and the acting chair of the IEEE Finland AP-03/ED-15/MTT-17 societies.

Tauno Vähä-Heikkilä (S'00–M'06) received the B.Sc. degree in space physics and M.Sc. degree in applied physics from the University of Turku, Turku, Finland, in 2000 and 2001, respectively, and the Dr. Tech. degree from the Helsinki University of Technology (TKK), Espoo, Finland, in 2006.

Since 2000, he has been with MilliLab, VTT Technical Research Centre of Finland, Espoo, Finland, where he is currently a Chief Research Scientist and Team Leader of adaptive radios. From 2002 to 2003, he visited The University of Michigan at Ann Arbor. He has authored or coauthored over 80 scientific publications. His research interests include technology, circuit, module, and architecture development for reconfigurable radios from handsets to millimeter-wave applications.